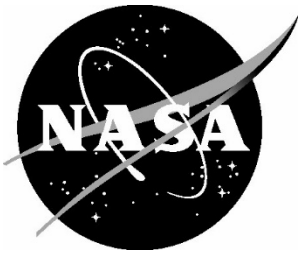
NASA/TM-20250009546



The HyMAP-3 Hydrodynamic Model

Augusto Getirana
NASA Goddard Space Flight Center, Greenbelt, MD
Science Applications International Corporation, Inc., Greenbelt, MD

Sujay V. Kumar
NASA Goddard Space Flight Center, Greenbelt, MD

Yeosang Yoon
NASA Goddard Space Flight Center, Greenbelt, MD
Science Applications International Corporation, Inc., Greenbelt, MD

Kristi R. Arsenault
NASA Goddard Space Flight Center, Greenbelt, MD
Science Applications International Corporation, Inc., Greenbelt, MD

James V. Geiger
NASA Goddard Space Flight Center, Greenbelt, MD

October 2025

NASA STI Program Report Series

Since its founding, NASA has been dedicated to the advancement of aeronautics and space science. The NASA scientific and technical information (STI) program plays a key part in helping NASA maintain this important role.

The NASA STI program operates under the auspices of the Agency Chief Information Officer. It collects, organizes, provides for archiving, and disseminates NASA's STI. The NASA STI program provides access to the NTRS Registered and its public interface, the NASA Technical Reports Server, thus providing one of the largest collections of aeronautical and space science STI in the world. Results are published in both non-NASA channels and by NASA in the NASA STI Report Series, which includes the following report types:

- TECHNICAL PUBLICATION. Reports of completed research or a major significant phase of research that present the results of NASA Programs and include extensive data or theoretical analysis. Includes compilations of significant scientific and technical data and information deemed to be of continuing reference value. NASA counterpart of peer-reviewed formal professional papers but has less stringent limitations on manuscript length and extent of graphic presentations.

- TECHNICAL MEMORANDUM. Scientific and technical findings that are preliminary or of specialized interest, e.g., quick release reports, working papers, and bibliographies that contain minimal annotation. Does not contain extensive analysis.

- CONTRACTOR REPORT. Scientific and technical findings by NASA-sponsored contractors and grantees.

- CONFERENCE PUBLICATION. Collected papers from scientific and technical conferences, symposia, seminars, or other meetings sponsored or co-sponsored by NASA.

- SPECIAL PUBLICATION. Scientific, technical, or historical information from NASA programs, projects, and missions, often concerned with subjects having substantial public interest.

- TECHNICAL TRANSLATION. English-language translations of foreign scientific and technical material pertinent to NASA's mission.

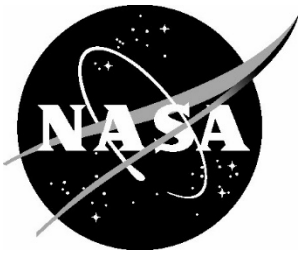
Specialized services also include organizing and publishing research results, distributing specialized research announcements and feeds, providing information desk and personal search support, and enabling data exchange services.

For more information about the NASA STI program, see the following:

- Access the NASA STI program home page at http://www.sti.nasa.gov

.

NASA/TM-20250009546



The HyMAP-3 Hydrodynamic Model

Augusto Getirana
NASA Goddard Space Flight Center, Greenbelt, MD
Science Applications International Corporation, Inc., Greenbelt, MD

Sujay V. Kumar
NASA Goddard Space Flight Center, Greenbelt, MD

Yeosang Yoon
NASA Goddard Space Flight Center, Greenbelt, MD
Science Applications International Corporation, Inc., Greenbelt, MD

Kristi R. Arsenault
NASA Goddard Space Flight Center, Greenbelt, MD
Science Applications International Corporation, Inc., Greenbelt, MD

James V. Geiger
NASA Goddard Space Flight Center, Greenbelt, MD

National Aeronautics and
Space Administration

NASA Goddard Space Flight Center
Greenbelt, MD

October 2025

The use of trademarks or names of manufacturers in this report is for accurate reporting and does not constitute an official endorsement, either expressed or implied, of such products or manufacturers by the National Aeronautics and Space Administration.

Available from:

NASA STI Program / Mail Stop 050
NASA Langley Research Center
Hampton, VA 23681-2199

Table of Contents

Table of Contents ..... *ii*
List of Tables ..... *iii*
List of Figures ..... *iv*
Abstract *1*
1. Introduction *2*
2. The Hydrological Modeling and Analysis Platform, version 3 ..... *3*
2.1. Water balance 3
2.2. River-floodplain interface 3
2.3. River and floodplain dynamics 4
2.4. Activating HyMAP-3 in LIS 6
2.5. Optimal time step for numerical stability 8
3. Advanced configurations *8*
3.1. Hybrid physics 8
3.2. Two-way coupling 9
3.3. Reservoir operations 10
3.3.1. Data-driven reservoir operation approach 10
3.3.2. Parameterized reservoir operation scheme 11
3.4. Bifurcation 12
3.5. Water management 13
3.6. Urban drainage scheme 14
3.7. Levees 17
3.8. Coastal interface 17
3.9. Beaver dams 20
4. Parameters *20*
5. Model outputs *22*
6. Upcoming capabilities *23*
6.1. SWOT data assimilation 23
6.2. Sediment transport 24
6.2.1. In-Channel Sediment Transport 24
6.2.2. Land-to-River Sediment Yield Module 24
6.2.3. Bed Stratigraphy and Layering 25
6.2.4. Numerical Implementation 25
6.2.5. Parameterization and Constants 25
References *26*
7. Supplementary Material *29*
7.1. Example of NetCDF file for the parameterized reservoir operation scheme 29
7.2. HyMAP-3 output attributes 30

List of Tables

Table 1. *Data-driven reservoir operation header file (RES_HEADER) format* *11*
Table 2. *Parameterized reservoir operation list file (RES_LIST) format* *12*
Table 3. *Bifurcation input file (BIF_INPUT_FILE) format* *12*
Table 4. *Water management input file (MANAG_INPUT_FILE) format* *13*
Table 5. *Urban drainage parameter file (URB_FILE_NAME) format* *15*
Table 6. *Coastal interface header file (SEA_LEV_HEADER) format* *18*
Table 7. *Outlet grid cell ID file (SEA_LEV_OUTLET) format* *18*
Table 8. *Beaver dam header file (SEA_LEV_HEADER) format* *20*
Table 9*. HyMAP-3 basic parameters* *21*
Table 10*. HyMAP-3 optional parameters* *22*
Table 11*. HyMAP-3 advanced parameters* *22*
Table 12. *HyMAP-3 output variables* *23*
Table 13*. List of sediment parameters* *25*

List of Figures

Figure 1. *Schematic of HyMAP-3's current capabilities. Connectors with arrows represent data flow when HyMAP-3 is coupled with external capabilities within LIS. Connectors without arrows represent HyMAP-3's internal capabilities* *3*
Figure 2. *Demonstration of HyMAP-3 output variables over the Tamsui River basin, in Northern Taiwan, at ~200-m spatial resolution.* *7*
Figure 3. *Panels on the left show impacts of two-way coupling over the Niger inner delta on spatially distributed (a) soil moisture and (c) surface water storage, at ~2-km spatial resolution. Impacts are defined here as the long-term difference between two-way and one-way coupling experiments, i.e., 2-WAY - 1-WAY. Panels on the right show monthly climatologies of corresponding spatially-averaged variables over flooding zones (source: Getirana et al., 2021)* *10*
Figure 4. *Schematic of the proposed urban drainage scheme within a squared 200×200-meter grid cell: (a) conceptual sub-grid representation of the urban drainage network, including the distribution of drain inlets and sub-grid cell inflow and outflow pathways (street block sizes are assumed as 100×100 meters); (b) conceptual representation of the street drainage and underground storm drain systems, including underground pipe width (W_d) gutter heigth (H_g) and width (W_g); and (c) conceptual drain inlet and its height (H_i) and width (W_i) (source: Getirana et al., 2023c)* *15*
Figure 5. *Preliminary implementation of HyMAP-3 over U.S. coasts. Blue stars represent NOAA tide gauges across five U.S. coastal areas: West Caribbean, East Caribbean, Northeast coast, Southeast coast, and West coast.* *19*
Figure 6. *Incremental flooded area over the Ganges-Brahmaputra Delta as a result of median flood events under the isolated influence of (a) vertical land motion, natural sea level variability, (c) sea level rise, (d) levees, (e) groundwater-fed irrigation and (f) all factors combined (source: Getirana et al., 2025)* *19*

Abstract

The Hydrological Modeling and Analysis Platform, version 3, (HyMAP-3) is a state-of-the-art global hydrodynamic model integrated into NASA's Land Information System (LIS; Kumar et al., 2006). HyMAP was initially developed in preparation for the Surface Water and Ocean Topography (SWOT) mission, where the objective was to have a modeling system capable of assimilating SWOT data toward a near-real-time global estimation of water discharge. Since the initial HyMAP implementation in 2011 (Getirana et al., 2012), HyMAP-3 has undergone numerous improvements, such as its vectorization and parallelization, inclusion of human and nature-driven processes (e.g., river damming, water management, river bifurcation, compound coastal flooding), full integration into LIS, and coupling with a wide range of land surface models (LSMs), data assimilation (DA) and forecast schemes. This technical memorandum fully describes HyMAP-3's concepts and capabilities, as well as its overall architecture within LIS.

1. Introduction

The Hydrological Modeling and Analysis Platform (HyMAP; Getirana et al., 2012) is a state-of-the-art, global-scale hydrodynamic model capable of simulating surface water dynamics, including water storage, extent, depth, flow velocity, and discharge in both rivers and floodplains. HyMAP was initially developed at *Laboratoire d'Etudes en Géophysique et Océanographie Spatiales* (LEGOS) and Meteo-France, in Toulouse, France, in the framework of the Surface Water and Ocean Topography (SWOT; Alsdorf et al., 2007; Getirana et al., 2024b) mission. The goal was to plan ahead of the upcoming satellite mission and have a global model capable of ingesting its inland water measurements towards improved estimates of global surface water dynamics (Getirana et al., 2012).

HyMAP was recoded, optimized, and integrated into NASA's Land Information System (LIS; Kumar et al., 2006) in 2011. Since then, multiple NASA-funded capabilities have been incorporated into the model, including a better representation of natural physical processes (e.g., accounting for backwater effects, coastal flooding, bifurcation), human interventions in river systems (e.g., reservoir operation, flood control structures, and urban drainage systems), full coupling with land surface models (LSMs) and irrigation schemes, integration with data assimilation (DA) schemes and forecast capabilities, and spatiotemporal flexibility. HyMAP version 3 (HyMAP-3) has evolved from the first HyMAP version as a result of the aforementioned improvements, all performed at NASA Goddard Space Flight Center (GSFC).

HyMAP-3 resolves the local inertia formulation unidimensionally (i.e., a unique flow direction is attributed to each grid cell). However, its capability of simulating backwater effects combined with interactions between rivers and floodplains and bifurcations (see below) results in a pseudo two-dimensional representation of surface water dynamics.

Previous HyMAP versions have been extensively evaluated in the Amazon basin (Getirana et al., 2013; Getirana and Peters-Lidard, 2013) and adopted as a tool for deltaic (Getirana et al., 2023a, 2021), regional (Getirana et al., 2014; Jung et al., 2017; Kumar et al., 2015, 2016) and global (Getirana et al., 2017a) water cycle studies. Today, HyMAP is used in numerous NASA projects, such as the North America Land Data Assimilation System, Version 3 (NLDAS-3; https://www.earthdata.nasa.gov/dashboard/stories/nldas), the NASA Hydrological Forecast Analysis System (NHyFAS; Arsenault et al., 2020) used in food and water security applications, and the NASA HydroGlobe (Nie et al., 2024). It has also been adopted by a wide range of U.S. and international institutions, including operational systems, such as U.S. Air Force's Global Hydro Information (GHI; https://www.nasa.gov/centers-and-facilities/jpl/nasa-soil-data-joins-the-air-force/), and Rio de Janeiro's Rio Flood Model (Rio-FM; Getirana et al., 2023b).

This technical memorandum fully describes HyMAP-3's concepts and capabilities available in LIS 7.7 and forward, entries needed to activate them and the model's arctecture within LIS. It is not the intent of this document to describe LIS or LIS capabilities associated with HyMAP-3, such as forecasting capabilities. That said, this document is intended to support HyMAP-3 users with basic knowledge on the LIS Framework, including the Land surface Data Toolkit (LDT; Arsenault et al., 2018), to become familiar with HyMAP-3 capabilities and how to use them within LIS. Details on access, compilation and use of the LIS Framework can be found on its GitHub page (https://github.com/NASA-LIS/LISF).

2. The Hydrological Modeling and Analysis Platform, version 3

This section explains the basic physical processes and options available in HyMAP-3. First, Sections 2.1-2.3 describe how the water balance and dynamics in rivers and floodplains are represented in the model. They are followed by a description of the options needed to activate HyMAP-3 in LIS, in Section 2.4. Finally, details about the model's numerical stability are provided in Section 2.5.

2.1.Water balance

HyMAP-3's main inputs are surface runoff and baseflow fields derived from the LSMs. When combined, these fields are also referred to as total runoff. The ingestion of total runoff data defines HyMAP-3's basic capability (Fig. 1 shows a schematic with HyMAP-3 capabilities), when the model is either one-way coupled with an LSM, or it reads in surface and baseflow fields from existing LSM outputs. Within a given HyMAP-3 grid cell draining a land surface with area A [m^2], the surface water storage, S [m^3], is defined by the continuity equation [Eq. (3)], and accounts for the total runoff generated over the time step, dt, as Qc_t [$m^3 \cdot dt^{-1}$] outflow, defined as both river and floodplain discharges to the downstream grid point, Q_t^r [$m^3 \cdot dt^{-1}$] and Q_t^f [$m^3 \cdot dt^{-1}$], and from the upstream grid cells, Qup_t^r [$m^3 \cdot dt^{-1}$] and Qup_t^f [$m^3 \cdot dt^{-1}$]:

$$S_{t+dt} = S_t + \left[Qc_t + \sum_{k=1}^{nUp}\left(Qup_t^{r,k} + Qup_t^{f,k}\right) - Q_t^r - Q_t^f\right] \cdot dt \qquad (1)$$

where superscripts r and f represent river channel and floodplain variables, respectively. dt [s] stands for the user-defined time step, and the index k counts the nUp upstream grid cells of the target grid cell.

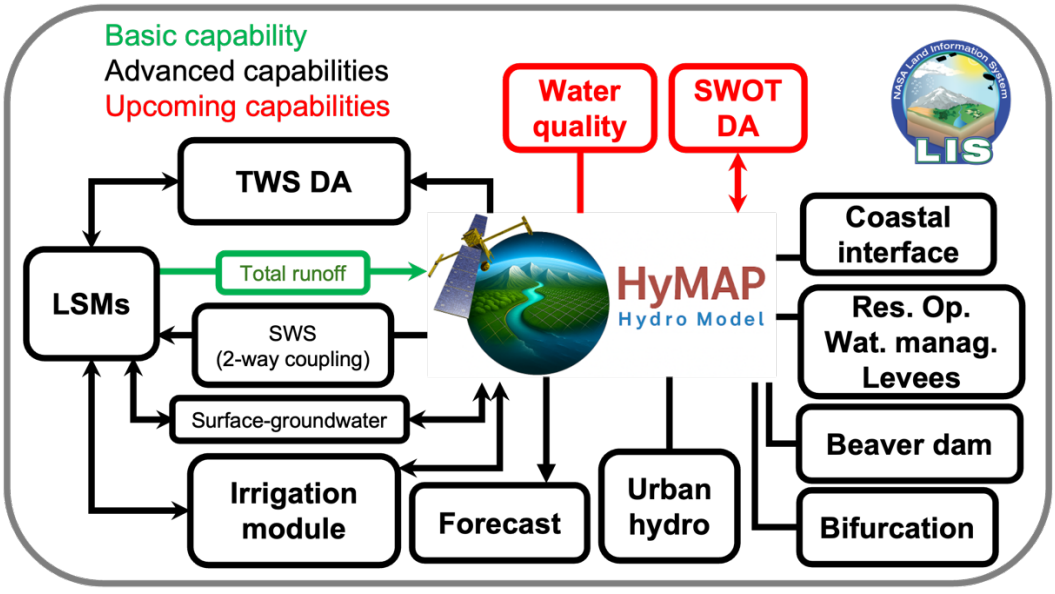


Figure 1. Schematic of HyMAP-3's current capabilities. Connectors with arrows represent data flow when HyMAP-3 is coupled with external capabilities within LIS. Connectors without arrows represent HyMAP-3's internal capabilities

2.2. River-floodplain interface

Rivers and floodplains interact laterally and have independent flow dynamics, with roughness and geometry derived from land cover characteristics, topography and river parameterization

(Getirana et al., 2013, 2012). Hypsographic curves, i.e., the relationship between water elevation (H) and storage (S) are derived from high resolution topographic data (see details in Section 5. Parameters). In addition to S, the flooded area (A) within a grid cell can also be determined through a relationship with H. As a result, floodplain water extent and storage can be derived from the floodplain water elevation with H×S×A relationships. If the water volume within a grid cell is above zero, the minimum A value corresponds to the river area (river length × river width) and it only increases once the river overflows to floodplains, with the grid area as the maximum value. The H×S×A relationship is derived for each grid cell from a pre-processing step where high resolution topography is upscaled to the model spatial resolution.

Water overflows to the floodplains when the river channel water height h_r [m] is higher than the bank height, H [m]. This process is considered instantaneous at each time step. This means that both the river channel and floodplain have the same water surface elevations. Elevation profiles are used to represent the depth-area-volume relationship in floodplains. As a result, floodplain water extent and storage can be derived from the floodplain water elevation, h_f.

The river and floodplain water exchange at each time step is represented as follows:

$$f\ S_{t+dt} \le S^{rmax}: \begin{array}{c} S^r_{t+dt} = S \\ h^r_{t+dt} = S^r_{t+dt}/(W \cdot L) \\ S^f_{t+dt} = 0 \\ h^f_{t+dt} = 0 \end{array} \tag{2}$$

$$else: \begin{array}{c} S^r_{t+dt} = S_{t+dt} - S^f_{t+dt} \\ h^r_{t+dt} = S^r_{t+dt}/(W \cdot L) \\ S^f_{t+dt} = \int_0^{A^f_{t+1}} \left[h^f_{t+dt} - h\left(A^f_{t+dt}\right)\right] dA \\ h^f_{t+dt} = h^r_{t+dt} - H \end{array} \tag{3}$$

where S_r [m^3] and S_f [m^3] stand for the river channel and floodplain water storages in the grid cell, h_r [m] and h_f [m] are the river and floodplain water depths, W [m] is the river width, L [m] is the river length, and A_f [m^2] is the flooded area. $S_{r\,\max}$ [m^3] stands for the river bankfull water storage, and is calculated as $S_{r\,\max}=H\times W\times L$.

2.3. River and floodplain dynamics

HyMAP-3 allows river and floodplain flow dynamics to be represented with either the kinematic wave equation or the local inertial formulation (or a combination of both, in hybrid mode). Both solutions consider rivers with a rectangular cross section and large width-to-depth ratio. The following option is needed in the LIS config file:

```
HYMAP3 routing method:  DYN_TYPE
```

where DYN_TYPE options are “kinematic”, “local inertia”, “hybrid”, and “urban”. More details on the hybrid and urban modes and options are provided in the Advanced Configurations section (Section 3).

Using the kinematic wave equation, river and floodplain flow velocities through a grid cell are

variable, and defined by the Manning equation simplified for rectangular, shallow channels, as follows:

$$v_{t+dt} = \frac{1}{n} \cdot {i_0}_t^{1/2} \cdot h_t^{2/3} \quad (4)$$

where v_{t+dt} [m·s^{-1}] is flow velocity at time step t+dt, n is the Manning roughness coefficient, and i_0 corresponds to the water surface elevation slope between the target and downstream grid cells. The kinematic wave option limits i_0 to positive values, with a minimum slope of 10^{-5} m·m^{-1}.

Water discharge Q_{t+dt} [m^3·s^{-1}] is the product of v and the flow area, defined as $W \times h_t$. Over floodplains, both W and h_t vary over time as a function of topographic characteristics within the grid cell described in section 3.2.

Local inertia solves the full momentum equation of open channel flow and accounts for a more stable and computationally efficient representation of river flow diffusiveness and inertia of large water mass of deep flow, which is essential for a physically-based representation of wetlands, lakes, floodplains, tidal effects and impoundments (Getirana et al., 2020). Following the explicit solution for the full Saint Venant equations presented in Bates et al. (2010) and improved in Almeida et al. (2012), the local inertia formulation can be defined for a rectangular, shallow channel as

$$Q_{t+dt} = \frac{Q_t + g \cdot h_t \cdot dt \cdot {i_f}_t}{\left(1 + g \cdot dt \cdot n^2 |\cdot Q_t| / h_t^{10/3}\right)} \quad (5)$$

where g is gravity, i.e., 9.81m·s^{-2}, and i_f is the water surface slope [m·m^{-1}].

HyMAP-3 can be run in hybrid mode, where both equations are used within a domain. In that case, a map determining the spatial distribution of flow types has to be provided (see section 3.3. Hybrid physics).

Rivers and floodplains flow independently from one grid cell to another, and have their hydrodynamics calculated separately using their own channel characteristics but using the same equations. At each time step, the average floodplain width, depth and bed height are defined as

$$\bar{W}_f = \frac{A_f}{L} \quad (6)$$

$$\bar{h}_f = \frac{S_f}{A_f} \quad (7)$$

$$\bar{z}_f = z_r + h_r - \bar{h}_f \quad (8)$$

For the kinematic wave equation, i_0 is considered the same for both rivers and floodplains. For most cases, river width W and bankfull height H are both defined based on empirical relationships with long-term average discharges, and the Manning coefficient of river channels n_r [-] varies as a function of H. The Manning coefficient for floodplains, n_f [-], is spatially distributed as a function of vegetation types derived from a static map (Masson et al., 2003), where larger values correspond to denser vegetated areas and lower values to sparser vegetated regions (see details in Section 4). Note that river geometry can be derived from ground measurements when available.

2.4. Activating HyMAP-3 in LIS

Prior to running HyMAP-3 within LIS, a model parameter input file is required to read in the key surfacetype, landmask, and HyMAP-3 suite of preprocessed model parameters. To process those parameters into a single, descriptive file (using netCDF format), LDT, which is part of the end-to-end LIS Framework, is run to read in and generate the final bundled parameter file, commonly named lis_input.nc. It typically contains the required dimensions, attributes, and parameters for running models, like HyMAP-3. This file is then loaded by LIS and the HyMAP-3 parameters are read in. For more information on the required and optional HyMAP-3 model parameters, please refer to the Section 4.

HyMAP-3's capabilities are options defined in a configuration file, referred to as LIS config file hereafter, which is used to specify runtime options for a given LIS simulation. Although parameters are generally provided on a gridded space, HyMAP-3 converts all 2-D input data to 1-D for vectorized and more efficient computations. This gives users the flexibility to adapt the model to vectorized parameters, such as those of the SWOT River Database (SWORD; Altenau et al., 2021). For the sake of simplicity, the model description will be based on grid-based domains.

HyMAP-3 can be executed in LIS through the config option below:

```
Routing model: "HYMAP3 router"
```

Three other options are required to define the time step, output and restart intervals:

```
HYMAP3 routing model time step:                "30mn"
HYMAP3 routing model output interval:          "1da"
HYMAP3 routing model restart interval:         "1mo"
```

Values provided above are suggestions and can be changed following LIS standards – please refer to the LIS Users Guide for details (https://nasa-lis.github.io/LISF/LIS_users_guide/LIS_users_guide.html).

River and floodplain flow dynamics are defined through the following option:

```
HYMAP3 routing method:  DYN_TYPE
```

where valid entries for DYN_TYPE are "kinematic", "local inertia", "hybrid", and "urban". More details on the hybrid and urban modes and options are provided in Section 3. Advanced Configurations.

Three additional options must be defined in the config file to set the ensemble mode, start mode and restart file path and name:

```
HYMAP3 run in ensemble mode: ENS_MODE
HYMAP3 routing model start mode: START_MODE
HYMAP3 routing model restart file: RESTART_FILE_NAME
```

ENS_MODE options are “0” for single member – or ensemble mean, if ensembles were turned on in the land surface model settings – simulation and “1” for ensemble simulation. If HyMAP-3 is used in an ensemble simulation, the model will adopt the same ensemble size set for the LSM. START_MODE can be set as “coldstart” or “restart”. If “coldstart” is used, rivers and floodplains in HyMAP-3 are initialized with zero storage. If “restart” is used, a restart path and filename (RESTART_FILE_NAME) must be provided.

Along with the appropriate parameter set provided in the lis_input.nc file, these are the basic config options to execute HyMAP-3 in LIS. Additional settings provided below are optional and used to either overwrite default configurations or activate advanced HyMAP-3 options.

The floodplain dynamics, as described in Section 2.3, must be activated through the following option in the LIS config file:

```
HYMAP3 floodplain dynamics: FLD_DYN
```

where FLD_DYN options are “1” to activate the floodplain dynamics, and “0” to deactivate it. If the latter is used, the floodplain behaves as a simple reservoir. In that case, water flows in and out to its corresponding river reach and is not exchanged with upstream and downstream grid cells.

Fig. 2 shows some HyMAP-3 output variables (i.e., streamflow, water surface elevation, surface water storage, flooded fraction, flow velocity and river depth) over the Tamsui River basin, in Northern Taiwan, at ~200-m spatial resolution. This simulation used used the local inertia formulation, adaptive time step and alpha value of 0.5, and floodplain dynamics. HyMAP-3 was coupled with the Noah-MP LSM (He et al., 2023) forced with NASA’s Modern Era Retrospective-Analysis for Research and Applications, version 2 (MERRA-2 ; Gelaro et al., 2017). The simulated domain is composed of 147,117 grid cells, and one day of simulation takes 2 minutes with 48 processors.

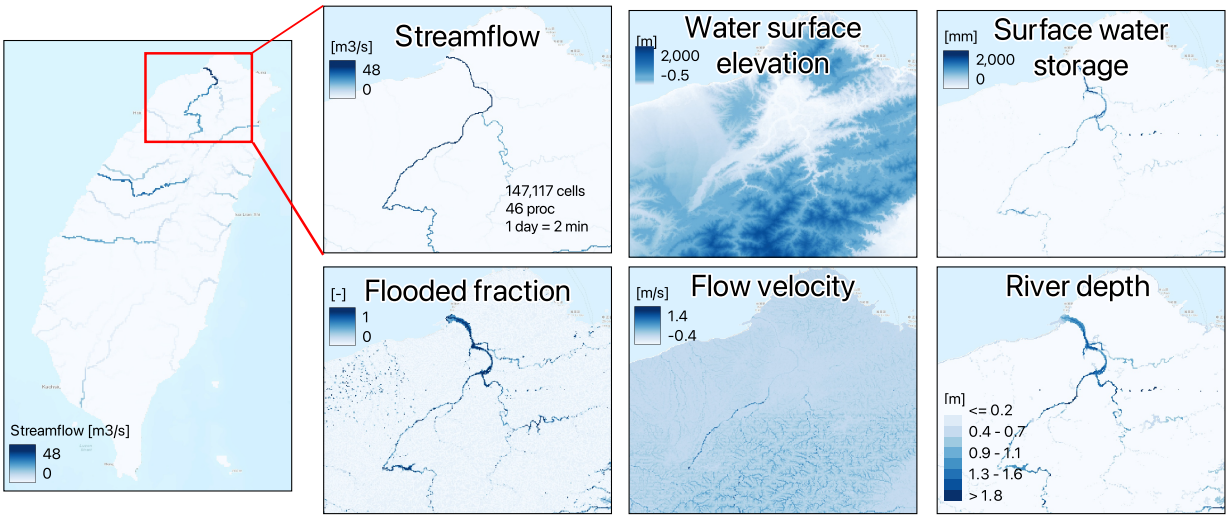


Figure 2. Demonstration of HyMAP-3 output variables over the Tamsui River basin, in Northern Taiwan, at ~200-m spatial resolution.

2.5. Optimal time step for numerical stability

Numerical stability can be achieved by breaking the user-defined time step (e.g., 15 min), as described in the previous section, into sub time steps. The Courant–Friedrichs–Levy (CFL) condition can be used to determine HyMAP-3's optimal sub time steps:

$$C_r = \frac{V \partial t}{\partial x} \quad (9)$$

where C_r stands for the non-dimensional Courant number and V is a characteristic velocity [$m \cdot s^{-1}$]. Numerical stability is obtained when C_r is less than 1. V can be defined for the local inertial form of the shallow water equations as (Bates et al., 2010):

$$V = \sqrt{gh} \quad (10)$$

Eq. (10) can be rewritten as follows, defining the maximum time step needed to keep numerical stability:

$$dt_{max} = \alpha \frac{dx}{\sqrt{g h_t}} \quad (11)$$

where α is a coefficient that is used to ensure that the selected time step remains, at all times, smaller than the maximum threshold for stability. Eq. (11) has been implemented in HyMAP-3 to determine optimal time intervals.

HyMAP-3 is set up as adaptive with α=0.5 (i.e., the actual time step used is 50% of the theoretical maximum) by default. The options below can be included in the LIS config file to customize the model. Time step options can be defined as "constant" or "adaptive" and are defined using the following option:

```
HYMAP3 routing model time step method: "adaptive"
```

If "constant" is used, HyMAP-3 will run with the user-defined model time step. If "adaptive" is used instead, an alpha coefficient value can be provided, if different than the default value, as follows:

```
HYMAP3 routing model adaptive time step alpha coefficient:
                        ALPHA_COEF
```

where ALPHA_COEF is the α value. Note that lower values tend to shorten sub time steps, decreasing numerical instability and increasing computational costs.

3. Advanced configurations

This section provides details on the advanced configurations available in HyMAP-3. They include: 3.1. Hybrid physics; 3.2. Two-way coupling; 3.3. Reservoir operations; 3.4. Bifurcation; 3.5. Water management; 3.6. Urban drainage; 3.7. Levees; 3.8. Coastal interface; and 3.9.Beaver dams.

3.1. Hybrid physics

A hybrid physics option is available in HyMAP-3, meaning that users can spatially combine the

kinematic wave equation and local inertia formulation. The following option is needed in the LIS config file:

```
HYMAP3 routing method:  "hybrid"
```

For HyMAP-3 to be used in hybrid mode, a map determining the spatial distribution of flow types must be provided as an additional parameter in the lis_input file, "HYMAP_river_flow_type", where local inertia and kinematic wave are classified as 1 and 3, respectively. Only grid cells classified as local inertia are considered in the computation of optimal time steps for numerical stability, which can be useful in optimizing computational costs with minimal loss of accuracy (Getirana et al., 2017b).

The approach described in Getirana and Paiva (2013) to classify flow types requires an initial 2-3-year simulation with the local inertia formulation across the domain to generate parameters, such as mean streamflow, river slope, flow velocity, river depth and time of peak (i.e., averaged time, in days, that it takes for a flood wave at a given river reach to go from trough to peak).

3.2. Two-way coupling

Interactions between the LSMs and HyMAP in LIS are enabled in a generic manner using the standardized software tools and paradigms enabled by the Earth System Modeling Framework (ESMF; Hill et al., 2004). Briefly, at the end of each HyMAP-3 sub time step, the surface water storage (SWS) variable [mm] is converted to water flux [$mm \cdot s^{-1}$] as a function of the user-defined time step and created as an export state from HyMAP to the LSM. The LSM then employs it to update the soil surface states and fluxes in the following time step. Over a non-saturated soil, that additional water may infiltrate, increasing soil moisture and, subsequently, evapotranspiration. The increased water availability in the soil also impacts the energy balance, resulting in a drop in soil surface temperature. The remaining water flux is converted back to water volume and routed by HyMAP through the river network. As the exchange states are defined using generic ESMF objects, this design allows the configuration of any LSM within LIS for use with HyMAP without significant model development efforts. A detailed description of this capability can be found in Getirana et al. (2021).

```
HYMAP2 enable 2-way coupling: 1

HYMAP2 2-way coupling flooded fraction threshold: THRSHLD
```

The two-way coupling capability is currently implemented with a simplified representation of land-surface water interface, i.e., it does not represent the heterogeneous surface and sub-surface water availability within a model grid cell. Instead, a single, but representative vertical column of surface water and soil type and moisture is assumed. As a result, a flooded fraction threshold value (THRSHLD) must be provided in order to trigger the two-way coupling. Flooded fraction varies from zero to 1, representing the grid area covered with water. If a given grid cell flooded fraction exceeds the threshold, the two-way coupling scheme assumes that the area is entirely flooded, and computes the surface water-land-atmosphere interactions accordingly. Due to this limitation, this capability is best suited for finer resolution applications (e.g., 2km or finer). An application over the Niger inner delta, in West Africa, at ~2-km resolution, used a flooded fraction threshold of 0.2 (Getirana et al., 2021). Fig. 3 shows the impact of two-way coupling on soil moisture and surface water storage.

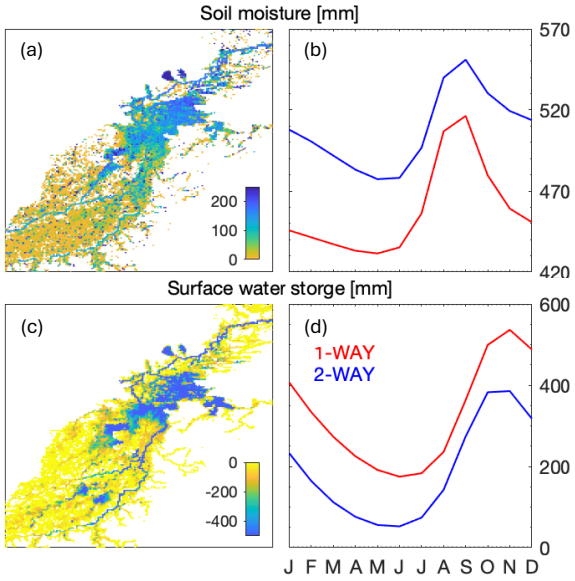


Figure 3. Panels on the left show impacts of two-way coupling over the Niger inner delta on spatially distributed (a) soil moisture and (c) surface water storage, at ~2-km spatial resolution. Impacts are defined here as the long-term difference between two-way and one-way coupling experiments, i.e., 2-WAY - 1-WAY. Panels on the right show monthly climatologies of corresponding spatially-averaged variables over flooding zones (source: Getirana et al., 2021)

3.3. Reservoir operations

HyMAP-3 can represent reservoir operations through two distinct ways: a data-driven approach and a parameter-based approach. The latter is based on Yassin's et al. (2019) methodology.

3.3.1. Data-driven reservoir operation approach

The data-driven reservoir operation scheme was designed to integrate radar altimetry data as a proxy of the reservoir operation rules. In this module, altimetric data informs HyMAP-3 on the actual reservoir water levels, which, in turn, combined with a DEM-based floodplain elevation profile, can be coonverted into the actual reservoir water storage through the hypsographic curve ($H \times S$). As described in Getirana et al. (2020a), the approach represents reservoir operations as follows: once identified as grid cell i where the dam is located, the observed water elevation (H_{obs}) at time step t is determined by a temporal linear interpolation of available radar altimetry observations. The temporal interpolation is performed within HyMAP-3. At the end of t, after the model simulates the naturalized downstream elevation (H_o), outflow (Q_o) and storage (S), the differential water storage, dS, needed to fill or empty i is determined by subtracting S from the satellite-based storage derived from the combination of H_{obs} with the hypsographic curve. Then, the following rule is applied to obtain the updated water storage (S'), elevation (H'_o) and outflow (Q'_o) at grid cell i and time step t:

$$if\,(Q_o - Q_{min}) \cdot dt \geq dS: \quad \begin{matrix} S' = S + dS \\ Q'_o = Q_o - (dS/dt) \\ H'_o = H_{obs} \end{matrix} \qquad (12)$$

$$S' = S + (Q_o - Q_{min}) \cdot dt$$
$$else\ if (Q_o - Q_{min}) \cdot dt < dS: \quad Q'_o = Q_{min} \quad (13)$$
$$H'_o = f[S', (H \times S)]$$

where *dt* stands for the time step interval and Q_{min} is the user-defined minimum reservoir outflow.

Using the local inertia formulation, water elevation, storage and flow in upstream grid cells are backwatered in subsequent time steps, reproducing the temporally continuous and spatially distributed dynamics of the reservoir. Note that results will not be realistic if the reservoir operation module is used with the kinematic wave equation.

The following options are needed in the LIS config file to represent this reservoir operation approach in HyMAP-3:

```
HYMAP3 reservoir operation option: 1

HYMAP3 reservoir operation header filename: RES_HEADER

HYMAP3 reservoir operation input directory: RES_DIR
```

Where RES_HEADER is a text file containing the list of reservoirs accounted for in the domain, and RES_DIR is where text files with time series for each reservoir can be found. Below is the RES_HEADER format:

Table 1. Data-driven reservoir operation header file (RES_HEADER) format

nr	ntr			
$resID_1$	$resX_1$	$resY_1$	$resQmin_1$	$resType_1$
		⋮		
$resID_{nr}$	$resX_{nr}$	$resY_{nr}$	$resQmin_{nr}$	$resType_{nr}$

where the first row is composed of *nr* and *ntr*, standing for the number of reservoirs within the domain and the number of time steps that will be used in HyMAP-3, respectively. Note that *ntr* can be equal to or less than the actual number of time steps in the input files.

The following rows, totaling *nr* rows, contain the reservoir IDs (*resID*), reservoir grid cell locations (*resX* and *resY*), the minimum reservoir outflow (*resQmin*), and reservoir operation type (*resType*). *resType*=1 for human controlled reservoirs. Each *resID* must have its corresponding text file in RES_HEADER with same name (i.e., resID.txt). Text files are composed of two columns. Each row corresponds to a date (YYYYMMDD) and respective reservoir water elevation.

3.3.2. Parameterized reservoir operation scheme

The parameterized reservoir operation scheme in HyMAP-3 follows Yassin et al. (2019). Briefly, the parameterization assumes that a reservoir is composed of five storage zones (dead storage, critical storage, normal storage, flood storage and emergency storage) and each has different operation rules, as a function of current storage, inflow and month of the year.

```
HYMAP3 reservoir operation option: 2
```

```
HYMAP3 reservoir operation input file: RES_HEADER_NC

HYMAP3 reservoir list: RES_LIST
```

where RES_HEADER_NC is a NetCDF file containing reservoir parameters (Section 7.1 in Supplementary Material shows an example of the NetCDF file for Lake Powell) and RES_LIST is a text file containing the list of reservoirs. The text file has the following format:

Table 2. Parameterized reservoir operation list file (RES_LIST) format

nr			
$resID_1$	$resX_1$	$resY_1$	$ncID_1$
		⋮	
$resID_{nr}$	$resX_{nr}$	$resY_{nr}$	$ncID_{nr}$

Where *nr* stands for the number of reservoirs within the domain, *resID* the reservoir ID, *resX* and *resY* reservoir grid cell locations within the HyMAP-3 domain, and *ncID* is the reservoir ID in the NetCDF file.

3.4. Bifurcation

River bifurcation, a common process found in flat areas, particularly river deltas, is represented in HyMAP-3. Following the methodology described by Yamazaki et al. (2014), bifurcation channels are defined as a function of ground elevation differences between grid points and corresponding neighbors. The following options are needed in the LIS config file:

```
HYMAP3 river bifurcation: 1

HYMAP3 river bifurcation pathway file: BIF_INPUT_FILE
```

BIF_INPUT_FILE is the input file name, which is in a text format, structured as follows:

Table 3. Bifurcation input file (BIF_INPUT_FILE) format

nb	nd							
$bdph_1$	…	$bdph_{nd}$						
$bman_1$	…	$bman_{nd}$						
upX_1	upY_1	$downX_1$	$downY_1$	$bElv_1$	$bLen_1$	$bWth_{1,1}$	…	$bWth_{nd,1}$
				⋮				
upX_{nb}	upY_{nb}	$downX_{nb}$	$downY_{nb}$	$bElv_{nb}$	$bLen_{nb}$	$bWth_{1,nb}$	…	$bWth_{nd,nb}$

Where the first row is composed of *nb* and *nd*, standing for the number of bifurcations within the domain and the number of bifurcation elevation thresholds, respectively. The second row contains *bdph* values, which are the heights of bifurcation elevation thresholds. The third row contains *bman* values, which are the roughness coefficient at each bifurcation elevation thresholds. The following rows, totaling *nb* rows, contain the upstream grid cell location (*upX* and *upY*), the downstream grid cell location (*downX* and *downY*), the bifurcation elevation ($bElv_{nb}$) length (*bLen*), and width of each elevation threshold (*bWth*). All parameters, except the roughness coefficient, can be derived from DEM processing, as described in Yamazaki et al. (2014).

Bifurcations are computed with the local inertia formulation. However, to avoid numerical instability, water only flows from the upstream grid cell to the downstream grid cell.

3.5. Water management

Water management is defined here as a human-controlled water diversion from a water body to another. Note that reservoir operation is excluded from this definition of water management, as it is represented in an independent module in HyMAP-3 (see Section 3.3). The water management module requires grid points for the water source (i.e., water body where structures are located) and destination (i.e., nearest water body where water is transferred to) as well as the operation rules (Getirana et al., 2023a). Currently, water management rules at can be represented in HyMAP-3 by either linear or polynomial equations derived from regressions between reported water diversions and river discharge upstream of management structures.

```
HYMAP3 water management: 1

HYMAP3 water management header file: MANAG_FILE_NAME
```

MANAG_INPUT_FILE is the input file name, which is in a text format, structured as follows:

Table 4. Water management input file (MANAG_INPUT_FILE) format

nm									
upX_1	upY_1	$downX_1$	$downY_1$	$mtype_1$	$c1_1$	$c2_1$	…	$c11_1$	$c12_1$
				⋮					
upX_{nm}	upY_{nm}	$downX_{nm}$	$downY_{nm}$	$mtype_{nm}$	$c1_{1nm}$	$c2_{nm}$	…	$c11_{nm}$	$c12_{nm}$

Where *nm*, in the first row, stands for the number of water management structures within the domain. The following rows, totaling *nm* rows, contain the upstream grid cell location, i.e., where the water is diverted from (*upX* and *upY*), the downstream grid cell location, i.e., where the water is diverted to (*downX* and *downY*), the equation type (*mtype*) representing the management rules, and 12 coefficients (*c1-c12*) used in different forms, depending on the rules.

Currently, HyMAP-3 represents management rules in three different ways. The first two have been customized to represent flood control structures in the lower Mississippi River (Getirana et al., 2023a), and the third one to represent water use in the Upper Colorado River basin. They are:

mtype=1: This option assumes that the diverted water discharge Q_d [$m^3 \cdot s^{-1}$] is defined by up to two polynomial equations ($Q_d = a.Q^2 + b.Q + c$). Coefficients a, b, and c for each equation are defined in Table 4 as *c1-c3 and c4-c6*, respectively. Polynomial equations 1 and 2 are used in the model within three streamflow Q thresholds (*c7-c9*) - note that Q is the simulated streamflow at the upstream grid cell. *c7* and *c8* define minimum and maximum Q thresholds for equation 1, and *c8* and *c9* define minimum and maximum Q thresholds for equation 2. If water management is represented by a single equation, *c4-c6* and *c9* must be defined as -9999. When using this option, *c10- c12* must be defined as -9999. If Q is beyond the thresholds, Q_d=0.

$$if\ c8 < Q \geq c7:\ \ Q_d = 1\,.\,Q^2 + c2\,.\,Q + c3 \quad (14)$$

$$else\ if\ c9 \leq Q \geq c8:\ \ Q_d = c4\,.\,Q^2 + c5\,.\,Q + c6 \quad (15)$$

$$else: Q_d = 0 \quad (16)$$

The simulated streamflow at upstream and downstream grid cells are updated accordingly at each time step.

mtype=2: This option assumes that polynomial equations 1 and 2 define water discharge diverted during ascending and descending Q, respectively. Ascending Q is defined as current value is higher than the previous one, and descending Q is defined as the current value being lower than the previous one. This option represents water diversions with a minimum (*c7*) and maximum (*c8*) transfer capacity. It also gives the option to provide maximum (*c10*) and minimum (*c11*) Q thresholds for transfer to occur.

mtype=3: Prescribed monthly climatology of water consumption. This option assumes that water is subtracted from the river system and does not return. Coefficients (*c1* to *c12*) correspond to monthly water use in $m^3 \cdot s^{-1}$, and only upstream grid cells are updated. This option can be used to add water to the river system, if negative coefficient values are provided instead:

$$Q_{d_{mon}} = c_{mon} \quad (17)$$

where *mon* stands for the month of the year.

3.6. Urban drainage scheme

The urban drainage scheme accounts for a modified parameterization of channels, as a way to replace rivers with a urban drainage network within so-called urban grid cells. This means that urban runoff flows thorugh street gutters rather than rivers. The following options are needed in the LIS config file:

```
HYMAP2 routing method: "urban"

HYMAP2 urban drainage parameter file: URB_FILE_NAME
```

Similar to the "hybrid" mode, "urban" requires a HYMAP_river_flow_type map identifying grid cells where urban drainage is computed. In addition to classes 1 and 3 (please refer to Section 3.1. Hybrid physics), values 4 and 5 identify urban drainage grid cells with local inertia and kinematic wave surface water flow, respectively.

The urban drainage scheme also requires an additional parameter in the LIS input file, HYMAP_urban_drainage_outlet, identifying urban drainage outlets (see Section 4). Drainage outlets are located at the urban-no urban interface, representing the end of the drainage system connected to a water body (e.g., river, channel, coast). Such a map is composed of "0" and "1" values, corresponding to "no outlet" and "outlet", respectively.

URB_FILE_NAME is the gutter and drainage network parameter file name provided in a text format. The file structure and suggested parameter values are listed in as follows:

Table 5. Urban drainage parameter file (URB_FILE_NAME) format

```
#gutter parameters
0.5             # gutter width [m]
0.15            # gutter height [m]
0.0004          # gutter density [units·m-2]
2.0             # gutter water intake velocity [m·s-1]
#
#drainage network parameters
100.            # street block length [m]
0.5             # underground squared pipe width [m]
0.02            # drainage length density [m·m-2]
0.012           # Roughness coefficient for cement pipes [-]
0.003           # drainage system slope [m·m-1]
```

Gutter height, H_g [m], is assumed 0.1. Gutter width, W_g [m], is defined as 0.5% of the grid length:

$$W_g = 0.005 \cdot L_b \tag{18}$$

where L_b [m] stands for the street block size. This corresponds to W_g=0.5m for a hypothetical 100-meter street block.

Water intake is represented by drain inlets with parameterized dimensions, density over urban areas and water intake velocity. Based on these parameters, the model determines the water intake within a grid cell at each time step during a rain event. That water is transferred from the surface to an underground storm drain system (USDS) that is also parameterized. For simplicity, the USDS follows the urban surface flow directions. Water flows in the USDS until it reaches non-urban grid cells or the coast.

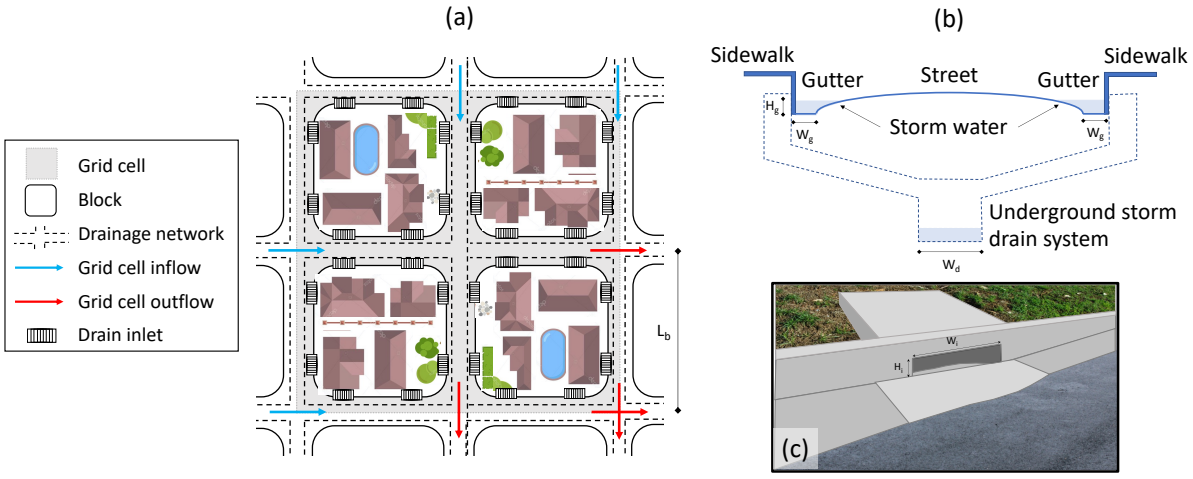


Figure 4. Schematic of the proposed urban drainage scheme within a squared 200×200-meter grid cell: (a) conceptual sub-grid representation of the urban drainage network, including the distribution of drain inlets and sub-grid cell inflow and outflow pathways (street block sizes are assumed as 100×100 meters); (b) conceptual representation of the street drainage and underground storm drain systems, including underground pipe width (W_d) gutter heigth (H_g) and width (W_g); and (c) conceptual drain inlet and its height (H_i) and width (W_i) (source:

Getirana et al., 2023c)

Sub-grid processes are simplified following the conceptual representations shown in Fig. 4. In the case of the underground drainage network, it is assumed that water storage within a grid cell is defined as the sum of all pipes draining the grid area. It is assumed an average squared street block size of L_b=100m and drainage length density, D_d [m·m^{-2}], of 0.02, corresponding to the presence of a single pipe across every street within the urban domain. It is also suggested a drain inlet density, D_i [units·m^{-2}], of 8×10^{-4}, corresponding to two drain inlets on each side of a 100-meter street. Drain inlet width and height are defined as W_i=1m and H_i=0.15m, respectively. Note, again, that all values are suggestions, following Getirana et al. (2023c), and can be changed as a function of the study case. The total drainage length, L_d [m], maximum water storage capacity in the USDS, $Smax_d$ [m^3], and number of drain inlets, N_i, within a grid cell are defined as:

$$L_d = D_d \cdot A_{grid} \tag{19}$$

$$Smax_d = w_d^2 \cdot L_d \tag{20}$$

$$N_i = D_i \cdot A_{grid} \tag{21}$$

where A_{grid} [m^2] is the grid cell area and w_d [m] the width of square-shaped underground pipes.

It is assumed w_d as one meter. As a result, a hypothetical 200×200m grid cell, with A_{grid}=40,000m^2, would be composed of four blocks, L_d=800m, N_g=32 drain inlets and $Smax_d$=800m^3. Also, as part of sub-grid simplifications, it is assumed that the number of USDS outlets N_{out} within a grid cell is defined as:

$$N_{out} = \frac{2 \cdot \sqrt{A_{grid}}}{L_d} \tag{22}$$

At each time step, urban drainage mass balance within a grid cell is defined as

$$S_{d_{t+dt}} = S_{d_t} + \left(I_{d_t} - Qout_{d_t} + \sum_{k=1}^{nUp} Qin_{d_{k,t}}\right) \cdot dt \tag{23}$$

where S_d [m^3] is the drainage water storage at time t [s], and dt stands for the model time step. Qin_d [m^3·s^{-1}] and $Qout_d$ [m^3·s^{-1}] are the drainage inflow and outflow, respectively. I_d [m^3·s^{-1}] is the urban surface vertical flow and the index k stands for the nUp upstream grid cells of the target grid point.

Vertical flow I_d occurs whenever there is water available on the urban surface or water excess in the USDS through a conceptialized dual drainage system (Schmitt et al., 2004), and is defined as

$$if\ S_{d_t} < Smax_d:\ I_{d_t} = N_g \cdot min\left(H_g, h_{s_t}\right) \cdot W_g \cdot v_g \tag{24}$$

$$if\ S_{d_t} \geq Smax_d:\ I_{d_t} = \left(Smax_d - S_{d_t}\right)/dt \tag{25}$$

where h_s [m] is the street water depth and v_g [m·s^{-1}] the water intake velocity. Although v_g is variable over time as a function of many factors, such as gutter and drain inlet shapes and surface water depth, it is assumed a constant value of 2 m·s^{-1}.

Water is routed across the USDS using the kinematic wave equation, considering a rectangular river cross section:

$$Qout_{d_t} = \frac{1}{n_d} \cdot i_d^{1/2} \cdot W_d \cdot h_{d_t}^{5/3} \quad (26)$$

where n_d [-] is surface roughness, i_d [m·m^{-1}] the drainage longitudinal slope, W_d [m] the total drainage width within a grid cell, defined as $W_d = N_{out} \cdot w_d$, and h_d [m] the drainage water depth. It is assumed n_d for concrete pipes as 0.012 (Chow, 1959) and a homogeneous slope i_d =0.003m·m^{-1} across the USDS. Section 4 summarizes all parameters used in the proposed urban drainage scheme.

At each time step, the remaining urban runoff that was not collected by the USDS is routed thorugh gutters using the local inertia formulation. If the water volume exceeds the gutter capacity, it overflows to streets and sidewalks. Flooded areas are defined by the fraction of streets and sidewalks within a grid that are covered with areas using a DEM-based hypsographic curve. Note that such a detailed flooding distribution is only possible with high-resolution DEMs (e.g., Lidar data) capable of detecting fine elevation differences at the street scale.

3.7. Levees

Levees are accounted for in HyMAP-3 by summing the levee height H_{lev} with the river bank height H, resulting in an increased $S_{r\ max}= (H+H_{lev})\times W\times L$, in Eq. (2). If river water storage exceeds $S_{r\ max}$, overflow occurs. Since there is a levee blocking direct interaction between floodplains and rivers, their water elevations may be different. Floodplain water returns to rivers when river height drops. Levees are included in the model through the option below:

```
HYMAP3 levee: 1
```

This option requires an additional parameter map in the lis_input.nc file, named HYMAP_levee_height, containing levee elevations in meters (see Section 4). Grid cells without levees should be flagged with zero value.

3.8. Coastal interface

By default, sea surface height (SSH) is assumed as zero across coasts and constant over time. With the local inertia formulation (see Section 2.3), backwater effects and seawater intrusion may occur, depending on inland water elevations. This means that water availability in the ocean is assumed unlimited and sufficient to flow inland whenever the model computes inflow (i.e., water flow from the ocean to the land/river areas). For example, in situations where river levels at outlets are below zero, water will flow from the ocean to the river. This may result in a mass imbalance, as the model "generates" water to represent ocean inflow into river systems. If the kinematic wave is used, river flow on coastal areas is constrained by a minimum positive slope.

HyMAP-3 also allows for a varying SSH in conjunction with the local inertia formulation. Previous studies have used weekly and daily radar altimetry data over oceans to represent SSH (Getirana et al., 2024a, 2023a). Because radar altimetry data does not represent near-coastal sub-daily processes, such as storm surges and tides, the use of sub-daily ground measurements, if available, is recommended. A more recent application used NOAA's tidal measurements at 10 locations to represent the spatiotemporal tidal variability over the Chesapeake Bay at 1-km spatial resolution. 10-min time step measurements were resampled to represent sub-daily high and low tides.

Coastal flooding can be represented in HyMAP-3's through the use of SSH data as downstream

boundary conditions as a proxy for ocean dynamics. The following options are needed in the LIS config file:

```
HYMAP3 sea level: 1

HYMAP3 sea level input directory: SEA_LEV_DIR

HYMAP3 sea level header filename: SEA_LEV_HEADER

HYMAP3 sea level outlet list: SEA_LEV_OUTLET
```

where SEA_LEV_DIR is the directory where SSH data is found, SEA_LEV_HEADER is a text file containing the list of available gauges and SEA_LEV_OUTLET is a text file listing the outlet grid cells using gauge data as downstream boundary conditions. Tables 6 and 7 exemplify the formats of SEA_LEV_HEADER and SEA_LEV_OUTLET files, respectively:

Table 6. Coastal interface header file (SEA_LEV_HEADER) format

nsl
$slID_1$
.   .   .
$slID_{nsl}$

Where *nsl* stands for the number of gauges with sea level time series and *slID* is the gauge ID. Each *slID* must have its corresponding text file in SEA_LEV_HEADER with same name (i.e., *slID*.txt), and each text file is composed of two columns: date (YYYYMMDD) and data (sea surface height).

Table 7. Outlet grid cell ID file (SEA_LEV_OUTLET) format

nout	ntout	
$outID_1$	$outX_1$	$outY_1$
	. . .	
$outID_{nout}$	$outX_{nout}$	$outY_{nout}$

Where *nout* is the number of outlet grid cells controlled by sea level as downstream boundary conditions. *outID* is refers to the gauge ID listed in SEA_LEV_HEADER that controls a given grid cell. *outX* and *outY* are the outlet grid cell locations. Note that *ntout* can be equal to or less than the actual number of time steps in the sea level time series files.

Fig. 5 illustrates the initial implementation of HyMAP-3 over U.S. coasts at 1-km spatial resolution, where the blue stars represent NOAA tide gauges used as downstream boundary conditions across five U.S. coastal areas. Outlet grid cells use the nearest tide gauge as downstream boundary conditions.

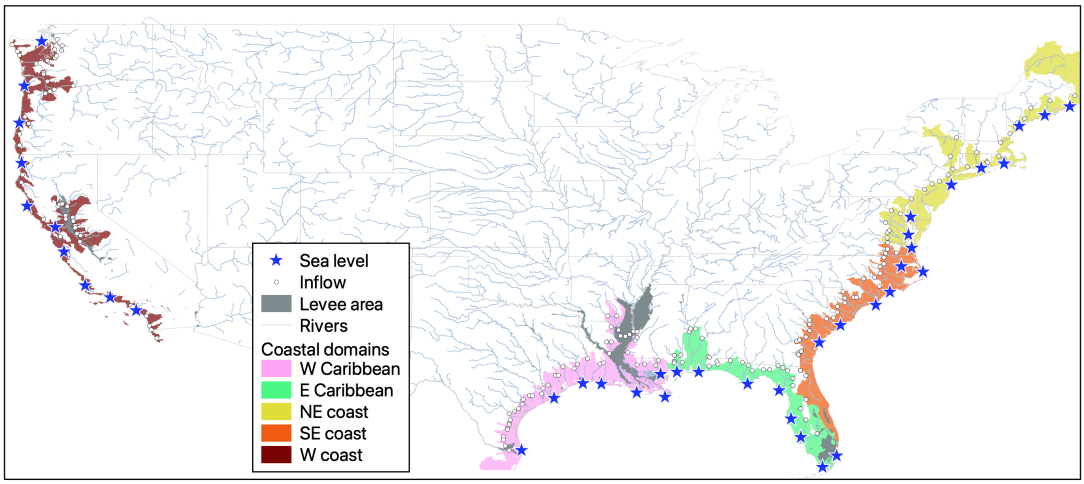


Figure 5. Preliminary implementation of HyMAP-3 over U.S. coasts. Blue stars represent NOAA tide gauges across five U.S. coastal areas: West Caribbean, East Caribbean, Northeast coast, Southeast coast, and West coast.

Finally, to exemplify the potential of different capabilities described so far, Fig. 6 shows the results from a recent study over the Ganges-Brahmaputra Delta at ~2-km spatial resolution, where HyMAP-3 was used to quantify the isolated impacts from multiple factors. Factors included vertical land motion, natural sea level variability, sea level rise, levees, irrigation, and all factors combined. Rather than varying the topography, vertical land motion was accounted for as sea level changes, keeping land static. Irrigation was accounted for through an irrigation scheme coupled with Noah-MP, which also assimilated satellite-based leaf area index data.

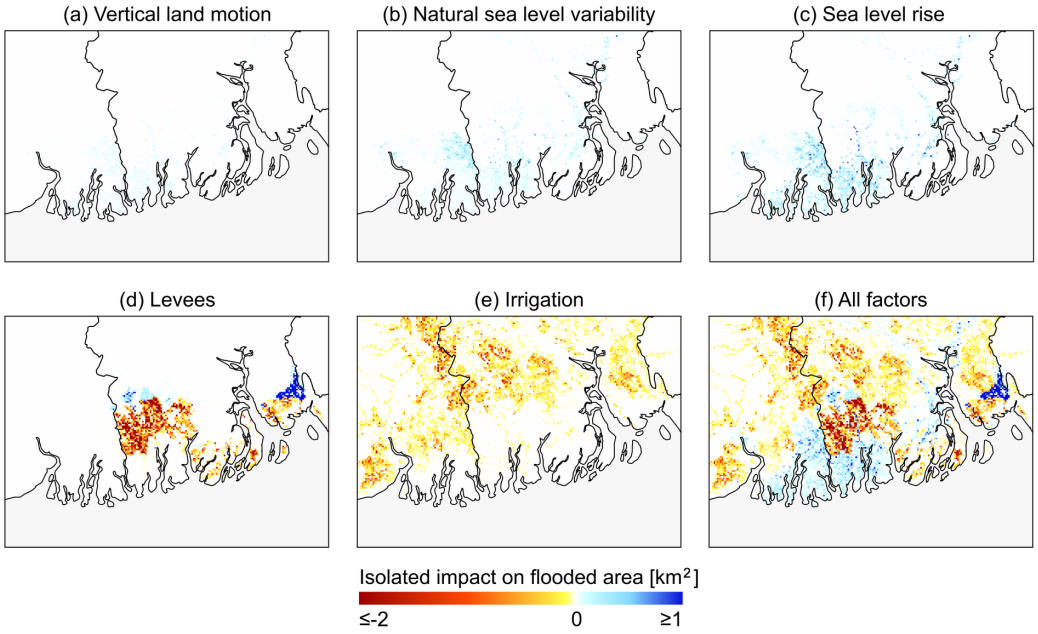


Figure 6. Incremental flooded area over the Ganges-Brahmaputra Delta as a result of median flood events under the isolated influence of (a) vertical land motion, natural sea level variability, (c) sea level rise, (d) levees, (e) groundwater-fed irrigation and (f) all factors combined (source:

Getirana et al., 2025)

3.9. Beaver dams

This module represents beaver dams as a cross-sectional levee with a leaking rate. If reservoir elevation exceeds dam height, water overflows. The following options are needed:

```
HYMAP3 reservoir operation option: 1

HYMAP3 reservoir operation header filename: BEAVER_HEADER

HYMAP3 reservoir operation input directory: BEAVER_DIR
```

The input file format is identical to that of the data-driven reservoir operation approach (Section 4.3.1), as follows:

Table 8. Beaver dam header file (SEA_LEV_HEADER) format

nr	ntr			
$resID_1$	$resX_1$	$resY_1$	$resQmin_1$	$resType_1$
		⋮		
$resID_{nr}$	$resX_{nr}$	$resY_{nr}$	$resQmin_{nr}$	$resType_{nr}$

Where, in the beaver dam module, *resQmin* is the leaking ratio, i.e., the inflow fraction that leaks through the beaver dam, varying from zero to 1. *resType*=2 for the beaver dams.

Each *resID* must have its corresponding text file in the BEAVER_DIR directory (files must be named as *resID*.txt) and listed in the BEAVER_HEADER file. Each text file is composed of two columns: date (YYYYMMDD) and data (beaver dam height). For constant beaver dam heights, a single row with any given date can be provided.

4. Parameters

HyMAP-3 parameters are generally derived from DEM processing and empirical equations. In most applications – particularly those at the global scale – river length, flow directions, elevation, floodplain height, grid distance, and grid and drainage areas are derived from the Flexible Location of Waterways (FLOW) upscaling method (Yamazaki et al., 2009) using the 90-meter resolution MERIT-Hydro dataset (Yamazaki et al., 2019) as input. Local DEMs can be processed and used in FLOW, when available (Getirana et al., 2023c). River geometry (width and height) and roughness coefficients can be derived from empirical equations following Getirana et al. (2012b). River geometry can also be based on spatial interpolation of ground observations, when sufficient data are available (e.g., Getirana et al., 2023b, 2023c). MERIT-Hydro also provides a global river width map, which can be used as an alternative.

Although parameters are usually provided on a gridded space, the HyMAP-3 code is vectorized. This means that the gridded input parameters are converted to vectors before the simulation starts. The main advantages of using gridded parameters are the easy coupling with land surface models (LSMs) and output visualization. However, future planned implementations will allow users to provide vectorized input parameters, such as SWORD (Altenau et al., 2021). The list of basic input parameters is provided in Table 9. Optional and advanced parameters can be found in Tables 10 and 11, respectively.

Table 9. HyMAP-3 basic parameters

Parameter ID	Unit	Description	Data types and inputs
HYMAP_river_width	m	Reach-averaged river width	-
HYMAP_river_height	m	Reach-averaged river full bank height	-
HYMAP_river_length	m	River length within grid cell	-
HYMAP_river_roughness	-	River roughness coefficient	Manning coefficient
HYMAP_floodplain_roughness	-	Floodplain roughness coefficient	Manning coefficient
HYMAP_flow_direction_x	-	Horizontal location of the downstream grid cell	Outlets are identified as -9
HYMAP_flow_direction_y	-	Vertical location of the downstream grid cell.	Outlets are identified as -9
HYMAP_grid_elevation	m	Grid cell elevation	Elevation at the grid cell outlet
HYMAP_floodplain_height	m	Grid cell height profiles above bankfull river elevation	This is a 10-layer parameter, each layer providing the equivalent height above 10% high-resolution DEM pixels; For example, layer 5 defines the elevation above 50% of high-resolution DEM pixels within the grid cell
HYMAP_grid_distance	m	Distance from a grid cell outlet to the next	-
HYMAP_grid_area	m^2	Grid cell area	-
HYMAP_basin_mask	-	Basin mask	Area within the domain where HyMAP-3 models surface waters (values >0)

Table 10. HyMAP-3 optional parameters

(not used in the model, but useful for output prost-processing)

Parameter ID	Unit	Description	Data types and inputs
HYMAP_node_lon	deg	Longitude at the grid outlet	Derived from high resolution DEM
HYMAP_node_lat	deg	Latitude at the grid outlet	Derived from high resolution DEM
HYMAP_drainage_area	m^2	Upstream drainage area	-
HYMAP_basin	-	Major basin delineation	-
Land_grid_area	m^2	Land model grid area	Area of the corresponding rectangular land grid cell

Table 11. HyMAP-3 advanced parameters

(needed in advanced model capabilities)

Parameter ID	Unit	Description	Observations
HYMAP_river_flow_type	-	Flow dynamic type	Required in hybrid and urban routing methods (Section 3.1 and 3.6, respectively); kinematic=1, local inertia=2-3; urban inertia=4; urban kinematic=5
HYMAP_urban_drainage_outlet	-	Urban drainage outlet	Required in the urban drainage module (Section 3.6); this map defines where urban drainage connects with surface waters
HYMAP_levee_height	m	Levee and poulder heights	Required in the levee module (section 3.7); this map defines heights added to the river bank that have to be reached before overflow to floodplains

5. Model outputs

HyMAP-3 output variables and their brief descriptions can be found in Table 12. Supplementary Section 7.2 provides the HyMAP-3 output list used in the model output attributes file (i.e., OUTPUT_LIST.TBL).

Table 12. HyMAP-3 output variables

Output ID	unit	Description
Streamflow	$m \cdot s^{-1}$	River + floodplain discharge
RiverStor	m	River water storage
RiverDepth	m	River depth
RiverVelocity	$m \cdot s^{-1}$	River flow velocity
FloodQ	$m \cdot s^{-1}$	Floodplain discharge
FloodStor	m	Floodplain water storage
FloodDepth	m	Floodplain average depth
FloodVelocity	$m \cdot s^{-1}$	Floodplain flow velocity
FloodedFrac	-	Grid cell flooded fraction [0-1]
FloodedArea	m^2	Grid cell flooded area
SurfElev	m	Surface water elevation
SWS	mm	Grid cell surface water storage
UrbDrainDis	$m \cdot s^{-1}$	Urban drainage discharge
UrbDrainStor	m	Urban drainage water storage

6. Upcoming capabilities

6.1. SWOT data assimilation

SWOT data assimilation has been implemented in LIS to work with HyMAP-3. HyMAP-3 assimilates SWOT-derived Water Surface Elevation (WSE) using the mission's Level-2 River Single-Pass Vector product as the observation source (see the SWOT data portal: https://podaac.jpl.nasa.gov/SWOT?tab=mission-objectives&sections=about%2Bdata). Rather than reading mission granules directly, observations are preprocessed into LIS-grid–aligned, daily datasets (global or regional). Each record retains its native timestamp but is grouped by day for efficient ingestion. Preprocessing applies quality control (mission flags and statistical outlier checks), maps observations to the corresponding HyMAP-3 river elements and performs vertical-datum harmonization (EGM2008 → EGM96) to ensure model–observation consistency.

The data assimilation method used as part of LIS is an Ensemble Kalman Filter (EnKF; Evensen, 1994), advancing ensemble members with the coupled land surface model and HyMAP-3. Updates occur whenever SWOT observations are available; the assimilation time

can be configured from the LSM's minimum time step (e.g., 15 minutes) up to daily cycles to meet operational needs. A topology-aware localization scheme – based on river-network connectivity and drainage-area relationships, rather than simple geographic distance – mitigates spurious correlations from limited ensemble sizes and yields physically consistent updates throughout the river network.

6.2. Sediment transport

A one-dimensional physically based sediment modeling framework is currently being implemented in HyMAP-3. The model prototype couples in-channel sediment transport with sediment yield from land, using a modular approach. Once integrated in HyMAP-3, it will run on the same spatial grid and will interface with land surface processes from LSMs (e.g., Noah-MP) through LIS. The model simulates sediment mass balance, stratigraphy, and grain class evolution across river segments, accounting for contributions from upstream reaches and land-derived inputs.

6.2.1. In-Channel Sediment Transport

Suspended sediment is modeled using the advection–diffusion–reaction equation:

$$\frac{\partial C}{\partial t} + u\frac{\partial C}{\partial x} = D\frac{\partial^2 C}{\partial x^2} + \frac{E - D_p}{H} \quad (27)$$

With C as depth-averaged sediment concentration [kg·m^{-3}], u is mean velocity [m·s^{-1}], D is sediment diffusivity [m^2·s^{-1}], H is water depth [m], and E and D_p are erosion and deposition rates [kg·m^{-2}·s^{-1}], respectively.

Bed elevation z_b evolves via the Exner equation:

$$\frac{\partial z_b}{\partial t} = \frac{D_p - E}{\rho_s(1-\lambda)} \quad (28)$$

with ρ_s as sediment density and λ the bed porosity. Each sediment grain class is independently tracked, with distinct settling velocities and critical shear thresholds based on Rijn (1984), García (2013), and Ariathurai and Arulanandan (1978).

6.2.2. Land-to-River Sediment Yield Module

A land sediment module is used to represent sediment inputs from hillslopes and land surfaces into river channels. Sediment generation is calculated using a formulation based on the Modified Universal Soil Loss Equation (MUSLE; Renard et al., 1997; Williams, 1975):

$$Y = R \cdot K \cdot C_f \cdot P \cdot LS \quad (29)$$

Where Y is sediment yield [kg·m^{-2}·s^{-1}], R runoff fluxes from LSM [kg·m^{-2}·s^{-1}], K soil erodibility factor [-], C_f: cover management factor, P support practice factor [-] and LS slope-length factor [-].

Runoff, as generated by LSMs, is used to estimate sediment yield per land grid cell, which matches the river grid in HyMAP-3. Sediment flux is distributed across grain size classes based on land-use-specific grain composition. These fluxes are introduced into the water column as a source term:

$$C_g \leftarrow C_g + \frac{Y_g \cdot \Delta t}{H} \quad (30)$$

where C_g and Y_g are the concentration and input rate of grain class g.

6.2.3. Bed Stratigraphy and Layering

The bed is represented using a two-layer stratigraphy: an active layer (typically 20% of the erodible thickness) and a substrate layer. The active layer interacts with the flow, exchanging sediment through erosion and deposition. When the active layer is exhausted, the substrate is promoted upward (Hirano, 1971). Each layer stores total thickness, dominant grain size, cohesion factor, and grain class composition (e.g., 30% clay, 40% silt, 30% sand). Erosion is halted when the bed reaches a user-defined minimum elevation (e.g., bedrock).

6.2.4. Numerical Implementation

All equations are discretized using an implicit finite difference scheme in space and time. Advection uses an upwind method, diffusion uses central differencing, and reaction terms (erosion/deposition) are treated semi-explicitly. The sediment concentration tridiagonal system is solved per grain class and time step. Time steps are dynamically adjusted based on both advection and diffusion Courant–Friedrichs–Lewy (CFL) criteria.

Land-derived sediment fluxes are applied before solving the in-channel transport. Bed updates are performed post-solution based on the erosion/deposition balance, and bed layer restructuring is handled as needed.

6.2.5. Parameterization and Constants

Table 13. List of sediment parameters

Parameter	Symbol	Value(s)	Units	Reference
Sediment density	ρ_s	2650	$kg \cdot m^{-3}$	Rijn (1984)
Water density	ρ_w	1000	$kg \cdot m^{-3}$	-
Grain diameters (clay–sand)	d	0.002, 0.02, 0.2	mm	García (2013)
Settling velocities	w_s	0.0001–0.002	$m \cdot s^{-1}$	Rijn (1984)
Diffusivity	D	0.05	$m^2 \cdot s^{-1}$	Calibrated
Erosion rate coefficient	M	5×10^{-7}	$kg \cdot m^{-2} \cdot s^{-1}$	Carey (1984)
Critical shear stress (erosion)	τ_{ce}	0.02–0.06	Pa	García (2013)
Critical shear stress (deposition)	τ_{cd}	0.015–0.045	Pa	García (2013)
Friction coefficient	F	0.03	–	Chow (1959)
Soil erodibility factor	K	0.02 (urban), 0.3 (pasture), 0.4 (cropland)	–	Renard et al. (1997)
Cover factor	C_f	0.01–0.9 (land-use-based)	–	Renard et al. (1997)
Practice factor	P	0.3–1.0	–	Wischmeier and Smith (1978)
Slope-length factor	LS	0.3–2.0	–	Wischmeier and Smith (1978)
Active layer fraction	–	0.2	–	Wilcock and Crowe (2003)

References

Almeida, G.A.M.D., Bates, P., Freer, J.E., Souvignet, M., 2012. Improving the stability of a simple formulation of the shallow water equations for 2-D flood modeling. Water Resources Research 48, 1–14. https://doi.org/10.1029/2011WR011570

Alsdorf, D.E., Rodrı´guez, E., Lettenmaier, D.P., Al, E., 2007. Alsdorf, D.E., Rodrıguez, E., Lettenmaier, D.P. 2007. Measuring surface water from space. Reviews of Geophysics, 45.pdf 1–24. https://doi.org/10.1029/2006RG000197.1.INTRODUCTION

Altenau, E.H., Pavelsky, T.M., Durand, M.T., Yang, X., Frasson, R.P. de M., Bendezu, L., 2021. The Surface Water and Ocean Topography (SWOT) Mission River Database (SWORD): A Global River Network for Satellite Data Products. Water Resources Research 57. https://doi.org/10.1029/2021WR030054

Ariathurai, R., Arulanandan, K., 1978. Erosion Rates of Cohesive Soils. Journal of the Hydraulics Division 104, 279–283. https://doi.org/10.1061/JYCEAJ.0004937

Arsenault, K.R., Kumar, S.V., Geiger, J.V., Wang, S., Kemp, E., Mocko, D.M., Beaudoing, H.K., Getirana, A., Navari, M., Li, B., Jacob, J., Wegiel, J., Peters-Lidard, C.D., 2018. The Land surface Data Toolkit (LDT v7.2) - A data fusion environment for land data assimilation systems. Geoscientific Model Development 11, 3605–3621. https://doi.org/10.5194/gmd-11-3605-2018

Arsenault, K.R., Shukla, S., Hazra, A., Getirana, A., McNally, A., Kumar, S.V., Koster, R.D., Peters-Lidard, C.D., Zaitchik, B.F., Badr, H., Jung, H.C., Narapusetty, B., Navari, M., Wang, S., Mocko, D.M., Funk, C., Harrison, L., Husak, G.J., Adoum, A., Galu, G., Magadzire, T., Roningen, J., Shaw, M., Eylander, J., Bergaoui, K., McDonnell, R.A., Verdin, J.P., 2020. The NASA hydrological forecast system for food and water security applications. Bulletin of the American Meteorological Society BAMS-D-18-0264.1. https://doi.org/10.1175/BAMS-D-18-0264.1

Bates, P.D., Horritt, M.S., Fewtrell, T.J., 2010. A simple inertial formulation of the shallow water equations for efficient two-dimensional flood inundation modelling. Journal of Hydrology 387, 33–45. https://doi.org/10.1016/j.jhydrol.2010.03.027

Carey, W.P., 1984. Physical Basis and Potential Estimation Techniques for Soil Erosion Parameters in the Precipitation-runoff Modeling System (PRMS). U.S. Geological Survey.

Chow, V. Te, 1959. Open Channel Hydraulics. McGraw-Hill, New York, New York, USA.

Evensen, G., 1994. Sequential data assimilation with a nonlinear quasi-geostrophic model using Monte Carlo methods to forecast error statistics. Journal of Geophysical Research: Oceans 99, 10143–10162. https://doi.org/10.1029/94JC00572

García, M.H., 2013. Sediment Transport and Morphodynamics 21–163. https://doi.org/10.1061/9780784408148.ch02

Gelaro, R., McCarty, W., Suárez, M.J., Todling, R., Molod, A., Takacs, L., Randles, C.A., Darmenov, A., Bosilovich, M.G., Reichle, R., 2017. The modern-era retrospective analysis for research and applications, version 2 (MERRA-2). Journal of climate 30, 5419–5454.

Getirana, A., Biswas, N.K., kumar, S., Nie, W., Ahmad, S., Maina, F.Z., Sakib, N., Hossain, M.S., Biswas, R.K., 2024a. Unsustainable groundwater-fed irrigation drives deltaic water scarcity and compound flooding. https://doi.org/10.21203/rs.3.rs-4355431/v1

Getirana, A., Boone, A., Yamazaki, D., Decharme, B., Papa, F., Mognard, N., 2012. The hydrological modeling and analysis platform (HyMAP): Evaluation in the Amazon basin. Journal of Hydrometeorology 13, 1641–1665. https://doi.org/10.1175/JHM-D-12-021.1

Getirana, A., Boone, A., Yamazaki, D., Mognard, N., 2013. Automatic parameterization of a flow routing scheme driven by radar altimetry data : Evaluation in the Amazon basin. Water Resources Research 49. https://doi.org/10.1002/wrcr.20077

Getirana, A., Dutra, E., Guimberteau, M., Kam, J., Li, H.Y., Decharme, B., Zhang, Z., Ducharne, A., Boone, A., Balsamo, G., Rodell, M., Toure, A.M., Xue, Y., Peters-Lidard, C.D., Kumar, S. V., Arsenault, K., Drapeau, G., Leung, L.R., Ronchail, J., Sheffield, J., 2014. Water balance in the amazon basin from a land surface model ensemble. Journal of Hydrometeorology 15, 2586–2614. https://doi.org/10.1175/JHM-D-14-0068.1

Getirana, A., Jung, H.C., Van Den Hoek, J., Ndehedehe, C.E., 2020. Hydropower dam operation strongly controls Lake Victoria's freshwater storage variability. Science of The Total Environment 726, 138343. https://doi.org/10.1016/j.scitotenv.2020.138343

Getirana, A., Kumar Biswas, N., Kumar, S., Nie, W., Ahmad, S., Maina, F., Sakib, N., Hossain, M.S., Biswas, R.K., 2025. Deltaic freshwater scarcity driven by unsustainable groundwater-fed irrigation. Nat Sustain. https://doi.org/10.1038/s41893-025-01566-0

Getirana, A., Kumar, S., Bates, P., Boone, A., Lettenmaier, D., Munier, S., 2024b. The SWOT mission will reshape

our understanding of the global terrestrial water cycle. Nat Water 2, 1139–1142. https://doi.org/10.1038/s44221-024-00352-0

Getirana, A., Kumar, S., Girotto, M., Rodell, M., 2017a. Rivers and Floodplains as Key Components of Global Terrestrial Water Storage Variability. Geophysical Research Letters 44, 10,359-10,368. https://doi.org/10.1002/2017GL074684

Getirana, A., Kumar, S., Konapala, G., Ndehedehe, C.E., 2021. Impacts of fully coupling land surface and flood models on the simulation of large wetlands' water dynamics: the case of the Inner Niger Delta. Journal of Advances in Modeling Earth Systems. https://doi.org/10.1029/2021MS002463

Getirana, A., Kumar, S., Konapala, G., Nie, W., Locke, K., Loomis, B., Birkett, C., Ricko, M., Simard, M., 2023a. Climate and Human Impacts on Hydrological Processes and Flood Risk in Southern Louisiana. Water Resources Research 59. https://doi.org/10.1029/2022WR033238

Getirana, A., Kumar, S., Konapala, G., Nie, W., Locke, K., Loomis, B., Birkett, C., Ricko, M., Simard, M., 2023b. Climate and Human Impacts on Hydrological Processes and Flood Risk in Southern Louisiana. Water Resources Research 59. https://doi.org/10.1029/2022WR033238

Getirana, A., Mandarino, F., Ney, P., Montezuma, D., Kirschbaum, D., 2023c. An urban drainage scheme for large-scale flood models. Journal of Hydrology 627, 130410. https://doi.org/10.1016/j.jhydrol.2023.130410

Getirana, A., Paiva, R.C.D., 2013. Mapping large-scale river flow hydraulics in the Amazon Basin. Water Resources Research 49. https://doi.org/10.1002/wrcr.20212

Getirana, A., Peters-Lidard, C., 2013. Estimating water discharge from large radar altimetry datasets. Hydrology and Earth System Sciences 17. https://doi.org/10.5194/hess-17-923-2013

Getirana, A., Peters-Lidard, C., Rodell, M., Bates, P.D., 2017b. Trade-off between cost and accuracy in large-scale surface water dynamic modeling. Water Resources Research. https://doi.org/10.1002/2017WR020519

He, C., Valayamkunnath, P., Barlage, M., Chen, F., Gochis, D., Cabell, R., Schneider, T., Rasmussen, R., Niu, G.-Y., Yang, Z.-L., Niyogi, D., Ek, M., 2023. Modernizing the open-source community Noah with multi-parameterization options (Noah-MP) land surface model (version 5.0) with enhanced modularity, interoperability, and applicability. Geoscientific Model Development 16, 5131–5151. https://doi.org/10.5194/gmd-16-5131-2023

Hill, C., DeLuca, C., Balaji, Suarez, M., Silva, A.D., 2004. The architecture of the earth system modeling framework. Computing in Science & Engineering 6, 18–28. https://doi.org/10.1109/MCISE.2004.1255817

Jung, H.C., Getirana, A., Policelli, F., McNally, A., Arsenault, K.R., Kumar, S., Tadesse, T., Peters-Lidard, C.D., 2017. Upper Blue Nile basin water budget from a multi-model perspective. Journal of Hydrology 555, 535–546. https://doi.org/10.1016/j.jhydrol.2017.10.040

Kumar, S., Peters-Lidard, C.D., Arsenault, K.R., Getirana, A., Mocko, D., Liu, Y., 2015. Quantifying the Added Value of Snow Cover Area Observations in Passive Microwave Snow Depth Data Assimilation. Journal of Hydrometeorology 16, 1736–1741. https://doi.org/10.1175/jhm-d-15-0021.1

Kumar, S.V., Peters-Lidard, C.D., Tian, Y., Houser, P.R., Geiger, J., Olden, S., Lighty, L., Eastman, J.L., Doty, B., Dirmeyer, P., Adams, J., Mitchell, K., Wood, E.F., Sheffield, J., 2006. Land information system: An interoperable framework for high resolution land surface modeling. Environmental Modelling and Software 21, 1402–1415. https://doi.org/10.1016/j.envsoft.2005.07.004

Kumar, S. V., Zaitchik, B.F., Peters-Lidard, C.D., Rodell, M., Reichle, R., Li, B., Jasinski, M., Mocko, D., Getirana, A., De Lannoy, G., Cosh, M.H., Hain, C.R., Anderson, M., Arsenault, K.R., Xia, Y., Ek, M., 2016. Assimilation of Gridded GRACE terrestrial water storage estimates in the North American land data assimilation system. Journal of Hydrometeorology 17, 1951–1972. https://doi.org/10.1175/JHM-D-15-0157.1

Masson, V., Champeaux, J.-L., Chauvin, F., Meriguet, C., Lacaze, R., 2003. A Global Database of Land Surface Parameters at 1-km Resolution in Meteorological and Climate Models. Journal of Climate 16, 1261–1282. https://doi.org/10.1175/1520-0442-16.9.1261

Nie, W., Kumar, S.V., Getirana, A., Zhao, L., Wrzesien, M.L., Konapala, G., Ahmad, S.K., Locke, K.A., Holmes, T.R., Loomis, B.D., Rodell, M., 2024. Nonstationarity in the global terrestrial water cycle and its interlinkages in the Anthropocene. Proceedings of the National Academy of Sciences 121, e2403707121. https://doi.org/10.1073/pnas.2403707121

Renard, K.G., Foster, G.R., Weesies, G.A., McCool, D.K., Yoder, D.C., 1997. Predicting Soil Erosion by Water: A Guide to Conservation Planning with the Revised Universal Soil Loss Equation (RUSLE), Agriculture Handbook No. 703. USDA.

Rijn, L.C. van, 1984. Sediment Transport, Part II: Suspended Load Transport. Journal of Hydraulic Engineering 110, 1613–1641. https://doi.org/10.1061/(ASCE)0733-9429(1984)110:11(1613)

Schmitt, T.G., Thomas, M., Ettrich, N., 2004. Analysis and modeling of flooding in urban drainage systems. Journal of Hydrology 299, 300–311. https://doi.org/10.1016/j.jhydrol.2004.08.012

Wilcock, P.R., Crowe, J.C., 2003. Surface-based Transport Model for Mixed-Size Sediment. Journal of Hydraulic Engineering 129, 120–128. https://doi.org/10.1061/(ASCE)0733-9429(2003)129:2(120)

Williams, J.R., 1975. Sediment-yield prediction with universal equation using runoff energy factor, in: Present and Prospective Technology for Predicting Sediment Yield and Sources. US Department of Agriculture, pp. 244–252.

Wischmeier, W.H., Smith, D.D., 1978. Predicting Rainfall Erosion Losses: A Guide to Conservation Planning. Department of Agriculture, Science and Education Administration.

Yamazaki, D., Ikeshima, D., Sosa, J., Bates, P.D., Allen, G.H., Pavelsky, T.M., 2019. MERIT Hydro: A High-Resolution Global Hydrography Map Based on Latest Topography Dataset. Water Resources Research. https://doi.org/10.1029/2019WR024873

Yamazaki, D., Oki, T., Kanae, S., 2009. Deriving a global river network map and its sub-grid topographic characteristics from a fine-resolution flow direction map. Hydrology and Earth System Sciences 13, 2241–2251. https://doi.org/10.5194/hess-13-2241-2009

Yamazaki, D., Sato, T., Kanae, S., Hirabayashi, Y., Bates, P.D., 2014. Regional flood dynamics in a bifurcating mega delta simulated in a global river model. Geophysical Research Letters 41, 3127–3135. https://doi.org/10.1002/2014GL059744

Yassin, F., Razavi, S., Elshamy, M., Davison, B., Sapriza-Azuri, G., Wheater, H., 2019. Representation and improved parameterization of reservoir operation in hydrological and land-surface models. Hydrology and Earth System Sciences 23, 3735–3764. https://doi.org/10.5194/hess-23-3735-2019

7. Supplementary Material

7.1. Example of NetCDF file for the parameterized reservoir operation scheme

NetCDF file summary: `resop_powell`

Dimensions

- **month:** 12 == Indicates the number of time points in the unit of months
- **res_count:** 1 == Reflects the number of reservoirs in this dataset

Global Attributes

- **missing_value:** -9999.f
- **description:** "Reservoir operation parameters following methodology in Yassin et al. (20019) https://doi.org/10.5194/hess-23-3735-2019"
- **institution:** "NASA GSFC"

Variable Summary

Variable	Dimensions	Units	Description
id	res_count	-	Reservoir ID
rank	res_count	-	Rank value to identify the grid cell as a reservoir
model_type	res_count	-	Model type (reservoir storage zone release)
lat	res_count	degrees	Latitudinal location of the reservoir (degrees)
lon	res_count	degrees	Longitudinal location of the reservoir (degrees)
max_sto	res_count	m3	Max reservoir capacity (m3)
init_dis	res_count	m3.s-1	Initial discharge (m3 s-1)
init_sto	res_count	m3	Initial storage (m3)
down_dis	res_count	m3.s-1	Downstream channel capacity (m3 s-1)
dead_sto	res_count	-	Dead storage fraction of maximum storage (0.1 means 10% of max storage)

rxn	res_count	m3	Random term variance or range (-)
mon_min_sto	month , res_count	m3	Monthly min storage (m3)
mon_nupper_sto	month , res_count	m3	Monthly normal upper storage (m3)
mon_upper_sto	month , res_count	m3	Monthly upper storage (m3)
mon_min_dis	month , res_count	m3.s-1	Monthly min release (m3 s-1)
mon_nupper_dis	month , res_count	m3.s-1	Monthly normal upper release (m3 s-1)
mon_upper_dis	month , res_count	m3.s-1	Monthly upper release (m3 s-1)
poly_a	res_count	-	Polynomial equation coef. a (y=ax^2 + bx +c)
poly_b	res_count	-	Polynomial equation coef. b (y=ax^2 + bx +c)
poly_c	res_count	-	Polynomial equation coef. c (y=ax^2 + bx +c)

7.2. HyMAP-3 output attributes

Streamflow: 1 m3/s - 1 0 0 1 333 10
RiverStor: 1 m3 - 1 0 0 1 333 10
RiverDepth: 1 m - 1 0 0 1 333 10
RiverVelocity: 1 m/s - 1 0 0 1 333 10
FloodQ: 1 m3/s - 1 0 0 1 333 10
FloodStor: 1 m3 - 1 0 0 1 333 10
FloodDepth: 1 m - 1 0 0 1 333 10
FloodVelocity: 1 m/s - 1 0 0 1 333 10
FloodedFrac: 1 - - 1 0 0 1 333 10
FloodedArea: 1 m2 - 1 0 0 1 333 10
SurfElev: 1 m - 1 0 0 1 333 10
SWS: 1 mm - 1 0 0 1 333 10
UrbDrainDis: 1 m3/s - 1 0 0 1 333 10
UrbDrainStor: 1 m3 - 1 0 0 1 333 10